Journal of Materials Chemistry A

Role of phosphate source in improving the proton conductivity of tin pyrophosphate and its composite electrolytes

Journal:	*Journal of Materials Chemistry A*
Manuscript ID	TA-ART-04-2020-004327.R1
Article Type:	Paper
Date Submitted by the Author:	26-Jun-2020
Complete List of Authors:	Ramaiyan, Kannan; University of New Mexico - Albuquerque, Herrera, Sergio; Sandia National Laboratories Workman, Michael; Los Alamos National Laboratory Semelsberger, Troy; Los Alamos National Lab, Atanasov, Vladimir; University of Stuttgart Kerres, Jochen; University of Stuttgart Maurya, Sandip; Los Alamos National Laboratory, MPA-11: Materials Synthesis and Integrated Devices Kim, Yu Seung; Los Alamos National Laboratory, Kreller, Cortney; Los Alamos National Lab, MPA11 Mukundan, Rangachary; Los Alamos National Laboratory, MPA-11

Role of phosphate source in improving the proton conductivity of tin pyrophosphate and its composite electrolytes

*Kannan P. Ramaiyan,[a] Sergio Herrera,[a] Michael J. Workman, [a] Troy A. Semelsberger, [a] Vladimir Atanasov,[b] Jochen Kerres, [b,c,d] Sandip Maurya, [a] Yu Seung Kim, [a] Cortney R. Kreller, [a] Rangachary Mukundan [a]**

[a]MPA-11, Los Alamos National Laboratory, Los Alamos, 87545, USA. E-mail: mukundan@lanl.gov
[b]Institute of Chemical Process Engineering, Boeblinger Str. 78, 70199 Stuttgart, Germany.
[c]Focus Area: Chemical Resource Beneficiation Faculty of Natural Sciences, North-West University, Potchefstroom 2520, South Africa
[d] Electrocatalytic Interface Engineering, Helmholtz Institute for Renewable Energies (HI-ERN), Egerlandstr. 3, 91058 Erlangen, Germany

Abstract

Metal pyrophosphates (MPP) in general and tin pyrophosphate (TPP) in particular have received significant interest in the last decade due to their potential as proton conductors for electrolyte application in intermediate temperature (IT)-fuel cells. However, for MPP based electrolytes, despite high reported proton conductivities, achieving good fuel cell performance and high Open circuit voltage (OCV) remains a challenge with synthesis methods playing a crucial role in determining the final proton conductivity. Here we report the role of phosphate precursor in determining the TPP proton conductivity by examining five different precursors including (1) - phosphoric acid (TPP-PA), (2) - ammonium hydroxide + phosphoric acid (TPP-NH_4OH), (3) - diammonium phosphate (TPP-DAP), (4) - tetramethylammonium sulphate + phosphoric acid (TPP-TMAP), and (5) - tetrabutylammonium phosphate (TPP-TBAP); where a maximum conductivity of 88 mS cm^{-1} at 200 °C was obtained for TPP prepared from TBAP precursor. TPP prepared from all different precursors formed the crystalline cubic Pa-3 phase after sintering at 650 °C for 2.5 hours. Further, TPP-TBAP/Nafion® composite membranes prepared with a 90:10

ratio exhibited an OCV of 0.98V and produced a maximum peak power density (PPD) of 630 mW cm^{-2} at an operating temperature of 220 °C. Our results demonstrate the significant impact of the TPP precursor on proton conductivity and fuel cell performance.

Introduction

Intermediate temperature (IT) fuel cells operating in the temperature range of 100 – 300 °C have been attracting increasing interest for more than a decade due to significant advantages over low temperature fuel cells such as; reduced catalyst poisoning, improved efficiency, easier water management and reduced use of noble metal catalysts.[1-4] Phosphoric acid doped polybenzimidazole (PBI) membranes are one of the most studied IT electrolyte, where the conductivity of the membrane increases with phosphoric acid doping.[5] For example, PBI membranes are reported to show proton conductivity of 46 mS cm^{-1} at 450% phosphoric acid doping that could be increased to 130 mS cm^{-1} at 1600 % of doping.[2] Further, the conductivity also depends on the membrane processing and morphology as membranes cast from polyphosphoric acid show higher conductivity than those cast from dimethylacetamide.[5] However, the operating temperatures of PBI-based PEMFCs are limited by the loss of the weakly bound phosphoric acid when fuel cells are exposed to water below 140 °C or operated above 200 °C.[6] Further, a tradeoff exists between the phosphoric acid uptake and mechanical stability of the membrane coupled with contamination of fuel cell components due to phosphoric acid leaching in highly doped membranes.

Recently, a variety of metal pyrophosphates (MP_2O_7, where M=Sn, Ti, Zr, W, Ce, Si, Ge) have been reported for intermediate temperature electrolyte applications following Hibino's reports on In doped tin pyrophosphate (ITPP) where $Sn_{0.9}In_{0.1}P_2O_7$ exhibited a proton conductivity of 195 mS cm^{-1} at 250 °C.[7-10] Recent studies on indium and other metal doped and undoped SnP_2O_7

have shown that the crystalline phase itself possesses negligible protonic conductivity (< 10^{-8} Scm^{-1} at 900 °C and < 10^{-11} Scm^{-1} at 600 °C) and the presence of an excess amorphous polyphosphate phase is the key for achieving high proton conductivities.[11, 12] For example, the proton conductivity of ITPP increased from 0.03 mS cm^{-1} to 10 mS cm^{-1} at 250 °C in dry nitrogen as the P:M ratio increased from 2.23 to 2.81.[13] The role of excess phosphate phase was further confirmed by experiments where phosphoric acid was utilized to recover the proton conductivity of TPP that was lost during high temperature sintering. For example, Li et al, enhanced the TPP proton conductivity from 0.9 mS cm^{-1} to 61 mS cm^{-1} by reacting the sintered TPP with PA.[14] Therefore in this paper we have concentrated on the conductivity of this amorphous phosphate rich phase whose conductivity could be as high as 10^{-1} Scm^{-1} at 250 °C. (Please add Ref 9 here, M. Nagao, A. Takeuchi, P. Heo, T. Hibino, M. Sano and A. Tomita, *Electrochemical and Solid-State Letters*, 2006, **9**, A105-A109).

To improve the proton conductivity further, a variety of acceptor dopants, both divalent and trivalent (In^{3+}, Al^{3+}, Mg^{2+}, Sb^{3+}, Sc^{3+}, and Ga^{3+}) have been tested where the maximum conductivity achieved remained at 195 mS cm^{-1} reported for $In_{0.1}Sn_{0.9}P_2O_7$.[2] Anionic conductivity in TPP materials was also reported when pentavalent Sb^{5+} or hexavalent Mo^{6+} were doped into SnP_2O_7. However, theoretical studies revealed that the hydroxide-ion exchange capability introduced via charge compensation was significantly lower than the reported anionic conductivity in these pentavalent and hexavalent doped TPPs.[15-17] For synthesizing the metal pyrophosphates, most of the reports utilize the method of reacting the precursor metal oxide powders with phosphoric acid and sintering at high temperatures from 650 – 1050 °C while new methodologies especially on heat treatment procedures are also being evaluated (M = Ce,[18, 19] Sb[20], Sn,[21-23], Ti,[24, 25] Zr,[26, 27]). Nevertheless, a major challenge in using metal pyrophosphate as electrolyte is forming

dense pellets and associated low open circuit voltages (OCV) and considerable gas crossover.[2] This could be due to their inability to form dense membranes (theoretical density =3.79 g cm^{-3}) in comparison to other ceramic electrolytes such as doped barium zirconates (6.21 g cm^{-3}) and yttria stabilized zirconia (6.05 g cm^{-3}).[28-30] For example, an OCV of 0.92 V is observed at 250 °C in comparison to the theoretical 1.1 V even for a 1.2 mm thick ITPP electrolyte.[9] Forming composites with suitable polymers helped to reduce the thickness of the electrolyte although the OCV remained poor even with a high polymer content (>70 wt%).[31, 32] For example, in an ITPP and sulfonated polystyrene-b-poly(ethylene/butylene)-b-polystyrene composite membrane based fuel cell with a 80:20 ceramic:polymer ratio, the OCV obtained at 200 °C was only about 0.8V. Further improvement in OCV was observed when PA was incorporated in the electrode layer that helped reduce the gas crossover across the membrane.[33] Our previous results on composite TPP/PFSA membranes also highlighted the challenge of low OCV, where OCV was ≈ 0.8 V in H_2/Air and ≈ 0.9 V in H_2/O_2 even though power densities as high as 870mW/cm^2 were achieve in O_2 at 240 ^oC.[34]

Recently, it was observed that the microstructure of SnP_2O_7 prepared by reacting SnO_2 with H_3PO_4 in air is very different from that of SnP_2O_7 prepared by reacting $SnCl_4$ with $(NH_4)_2HPO_4$ in water indicating a potential for improving the density of metal pyrophosphates.[7, 8, 35] Further, the synthesis history is reported to be important for achieving good proton conductivity as SnP_2O_7 prepared by an aqueous solution method showed negligible proton conductivity while the same material prepared by an acidic route showed very good conductivity.[35, 36] Our group has previously demonstrated synthesis of In doped TPP powders via a solution precipitation method that provided better control over the metal to phosphorous ratio than the traditional acidic route.[37, 38] However, no report is available on the role of phosphate

precursor in controlling the morphology, phosphoric acid uptake and proton conductivity. Hence, in this paper, we report the impact of the phosphate precursor structure on proton conductivity. We prepared TPP particles with five different phosphate precursors using an aqueous co-precipitation method. The evaluated precursors were (1) - phosphoric acid (PA), (2) - ammonium hydroxide + phosphoric acid (NH_4OH-PA), (3) - diammonium phosphate (DAP), (4) - tetramethylammonium sulphate + phosphoric acid (TMAP), and (5) - tetrabutylammonium phosphate (TBAP). We compare the proton conductivity of the resulting TPP powder in pellet form as well as in thin-film composite membrane form, fabricated with perfluorosulfonic acid (PFSA) ionomer in a weight ratio of 90:10 TPP:polymer, respectively. PFSA ionomer was chosen for its excellent elastic and composite forming properties with a variety of materials and partly due to difficulty in forming homogeneous membranes with PBI at TPP concentrations above 50%.[31, 34, 39] The fuel cell performance of these composite membranes is presented, highlighting the important role the phosphate precursor and phosphoric acid doping during the membrane casting process play in obtaining membranes with low gas crossover and high OCV.

Results and Discussion

TPP powders prepared from various phosphate precursors are characterized by x-ray diffraction (XRD) measurements for assessing their crystallinity and phase purity. The diffraction patterns of all the prepared powders are shown in Fig. 1 along with the diffraction pattern for the cubic Pa-3 symmetry structure (JCPDS (00-029-1352) of SnP_2O_7.[40] The lattice parameter ranged from 7.938 – 7.960 while the crystallite sizes varied from 28.2 – 43.6 nm. This is in agreement with previous reports from our group [13] as well as from literature [12] indicating the dominant role of sintering temperature in forming the crystalline phase, as precursors as well as preparation procedure were different for the prepared powders (See experimental Table 3). The lattice parameters obtained for

TPP derived from each starting material are given in Table 1 along with the P:M ratio and the measured pellet and membrane conductivities.

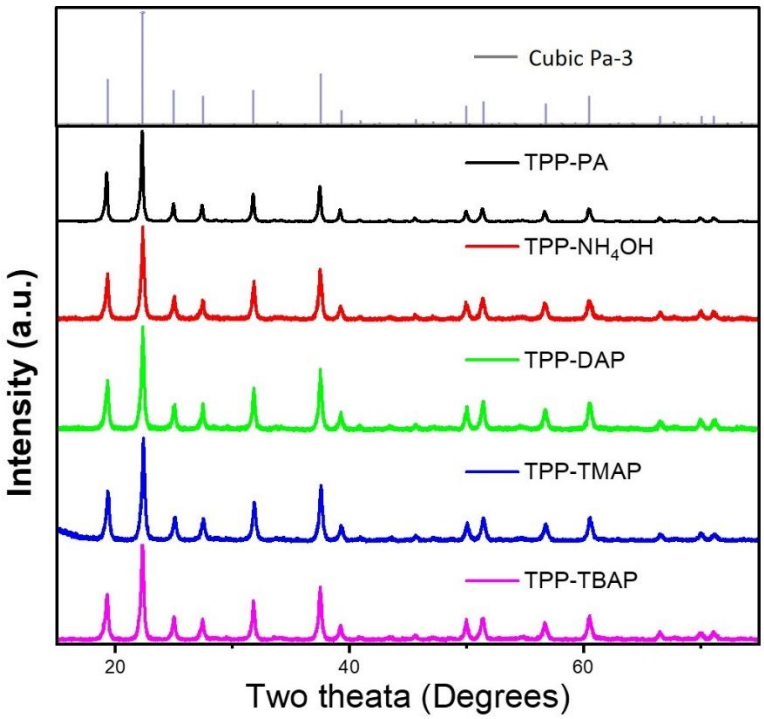

Fig. 1 XRD of the TPP powders obtained from different precursors after sintering at 650 °C for 2.5 hours along with the peak position reported for cubic Pa-3 system of SnP_2O_7.

Table 1 Crystallite size and lattice parameter obtained from XRD measurements after whole profile fitting along with P:M ratio obtained from TGA measurements and pellet conductivity measured at 200 °C and membrane conductivity measured at 220 °C by electrochemical impedance spectroscopy.

TPP powder	Crystallite size (nm)	Lattice Parameter (Å)	P:M ratio from TGA	Pellet conductivity (mS cm^{-1}) @ 200 °C	Membrane Conductivity (mS cm^{-1}@220 °C)
TPP-PA	43.6	7.960	3.11	80	45.0
TPP-NH_4OH	29.1	7.948	3.08	76	58.1
TPP-DAP	32.4	7.948	3.16	67	63.9

TPP-TMAP	28.2	7.938	2.62	6	NA
TPP-TBAP	30.1	7.947	3.02	88	94.8

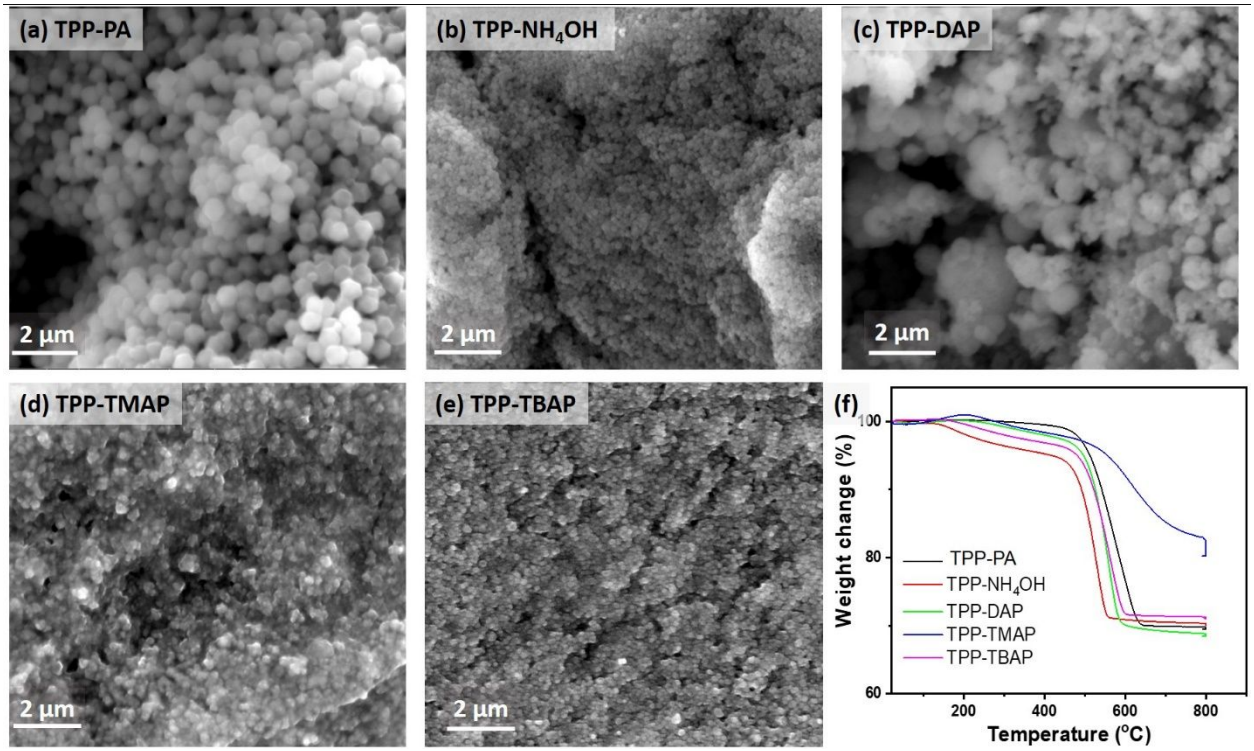

Fig. 2 (a – e) SEM images obtained for TPP powders prepared from five different precursors and (f) TGA of those TPP powders measured in air from 25 °C to 800 °C at a ramp rate 10 °Cmin^{-1}.

The surface morphologies of the prepared TPP powders are shown in Fig. 2a – 2e after sintering at 650 °C. The SEM images clearly indicate different morphologies with varying particle sizes. For example, TPP-PA that is prepared with no ammonium ions in the preparation procedure and having only oxalic acid has formed particles of close to 500 nm diameter size. The addition of oxalic acid that has a low decomposition temperature (~200 °C, Fig. S1) has helped form well defined particles. In the case of TBAP, where the hydrocarbon content is ~67% and decomposition is slow up to 500 °C, it has helped form significantly smaller particles with average size of ~160 nm. TPP-NH_4OH and TPP-TMAP both formed similar structural morphology with particle sizes close to 200 nm. However, TPPDAP where no hydrocarbon was present (no oxalic acid added)

showed widely varying particle sizes from 200 nm to 1 μm indicating that the addition of oxalic acid or inherent presence of hydrocarbon in the phosphate precursor, that decompose < 400 °C, helps to form well defined particles. The TGA of all the phosphate precursors are given in Fig. S1. The decomposition of the precursor in the temperature range 200 – 400 °C is critical to uniform particle size with higher decomposition temperatures providing smaller TPP particle sizes.

TPP powders prepared from methods (1) – (3) formed a white powder while (4) and (5) formed black and grey powders respectively (Fig. S2a) that could be attributed to the formation of carbon during sintering due to the high carbon content of the phosphate precursors; a process that may be similar to coking in solid oxide fuel cells.[41] However, the addition of oxalic acid in the preparation stage for the other two procedures did not affect the appearance of the powders as it has a very low decomposition temperature (< 200 °C).[42] A maximum total weight loss of 32% in the TGA was observed for TPP-DAP while the lowest of 20% was observed for TPP-TMAP after holding the samples at 800 °C for 1 hour. TPP-TMAP further showed a slow weight loss in the temperature range of 600 – 700 °C in contrast to the sharp weight loss around 550 – 600 °C for all other TPPs. This slow weight loss could be attributed to the combined loss of excess phosphate phase and carbon present in the material as evidenced by its black color (Fig. S2a) and the appearance of graphite oxide peak at a 2-theta value of 11.8° in its XRD data (Fig. S3).[43-45] All the samples became white in appearance after heating them to 800 °C indicating the removal of all carbon from the precursors (Fig. S2b). Nevertheless, all powders retained their crystallinity and no change was observed in pXRD (Fig. S4).

The TGA of the prepared powders shown in Fig. 2f demonstrates no significant weight loss up to 200 °C (<1%) indicating the possible suitability of these materials for electrolyte application in the

intermediate temperature range although this was observed at a faster heating rate. Between 200 – 450 °C, TPP powders prepared with ammonium-based precursors all show a small weight loss that could be attributed to the loss of residual ammonium ions that were not burned off during the sintering. TPP prepared with NH_4OH showed a maximum weight loss of 5% at 450 °C while TPP-PA synthesized with no ammonia precursors had a weight loss of less than 1% in this temperature range. To further confirm the presence of ammonium ions in the TPP powders, we tested the TPP powders for ammonia content by the indophenol method which further confirmed the ammonia content in the TPP powders in the following order DAP>NH_4OH>TBAP>TMAP>PA (See Fig. S5 and supporting information for the experimental methods).[46] Thus, clearly the precursors play a crucial role in the final morphology, impurity content and electronic property of the resulting TPP powder. In particular, TBAP due to its hydrocarbon content and higher decomposition temperature provides smaller and uniformly size distributed TPP particles.

Conductivity of the pellets

The conductivity of the pellets measured in a compression setup between two Pt electrodes are given in Table 1 along with the phosphorous to metal (P:M) ratio calculated from the TGA data. TPP-TMAP showed a low pellet conductivity of 6 mS cm^{-1}. While this material also had the lowest P:M ratio of 2.62, the low frequency impedance feature exhibited a depressed semi-circle corresponding to the low electrode interface resistance of mixed ionic electronic conductivity, in contrast to the low frequency capacitive feature observed for protonic conducting materials (Fig. S6). The mixed ionic-electronic conductivity is most likely due to the residual graphite oxide, as observed in its XRD (Fig. S3), and as the goal herein was to evaluate TPP materials as electrolytes, TPP-TMAP powders are not further discussed in the manuscript. TPP-TBAP showed a maximum pellet conductivity of 88 mS cm^{-1} at 200 °C with a P:M ratio of 3.02. There clearly is a correlation

between the particle size and pellet conductivity as despite having higher P:M ratios of 3.11 (TPP-DAP) and 3.16 (TPP-PA), these two samples with larger particle sizes exhibited lower pellet conductivities of 67 and 80 mS cm^{-1} respectively. TPP-TBAP despite a lower P:M ratio of 3.02 showed a higher pellet conductivity of 88 mS cm^{-1} that could be related to its smaller particle size forming denser pellets. The activation energy associated with this type of pellets are observed to be about 0.45 eV. The TGA of the precursor materials is shown in Fig. S1 indicating a complete decomposition temperature of 215 °C for oxalic acid while TBAP decomposes in the 200 -600 °C range. Since Oxalic acid burns off at a lower temperature, the particles are able to sinter and grow in size to the range of 450 – 500 nm. However, TBAP burns off at higher temperatures, and the resulting particles are both uniform and small in size (150 -175 nm). In contrast, in TPP-DAP, even though DAP burns off at a higher temperature than oxalic acid, there is no HC present in the precursor so the result is a wider range in particle size from few hundred nanometers to few microns. These results, further iterate the importance of carefully choosing the precursors to obtain TPP with higher conductivity.

TPP-Nafion composite membranes

TPP-Nafion® composites were fabricated by mixing 1.35 g of TPP powder with 3.00 g of 5 wt% Nafion® solution in 1,2 pentanediol to get a TPP:Nafion® ratio of 90:10. During the slip formation, 0.9 g of 85% phosphoric acid was added as a plasticizer as well as doping agent. The addition of PA was critical in preparing a thick slurry and achieving membranes with homogeneous distribution of TPP and Nafion®, as seen in their cross-sectional SEM images shown in Fig. 3a – 3d. The visible porosity in SEM images of the prepared membranes decreased with increasing cation size of ammonium ion precursor or the resultant particle size (TPP-PA<NH_4OH<DAP<TBAP). This was further confirmed via porosity measurements from the SEM

images by ImageJ® software, developed at the National Institute of Health, where the area of pores was measured by forming a binary image (Fig. S7). Through this analysis, we observed a maximum porosity of 35.26% for TPP-PA/Nafion® composite membrane and a minimum porosity of 4.19% for TPP-TBAP/Nafion® membranes (Fig. S7). We further attempted to measure the porosity of TPP-PA/Nafion® and TPP-TBAP/Nafion® by mercury intrusion porosimetry (MIP), where measured samples exhibited total intrusion less than 7%. When intrusion at low pressures that would correspond to spaces between the individual powder particles are excluded, total intrusion for all samples was below 1%. Membranes that show porosity in the several micron range by SEM show no porosity between 0.5 - 25 μm by MIP. We believe that the mismatch between the pores observed by SEM and those measured by MIP can be attributed to the compressibility of these materials (Fig. S8). The addition of PA during slip formation is essential for forming homogeneous membranes as TPP-Nafion® membranes prepared from slips without PA addition seem to segregate and form polymer rich and ceramic rich layers (Fig. S9). No segregation of ceramic and polymer layer was observed when PA is added during the slip formation as evidenced by their SEM images (**Fig.** 3a – 3d). Further, PA doping after forming these membranes does not provide the same level of PA incorporation as even after five days of imbibing in 85% PA, the PA uptake is only half of the 30% achieved by adding PA during the slip formation as evidenced by their TGA plots (Fig. S10). This could possibly be due to the use of acidic Nafion® as binding polymer that does not uptake PA as easily as polybenzimidazole based membranes.[47]

The TGA of the TPP-Nafion® composite membranes prepared with PA as plasticizer is shown in Fig. 3e. All the membranes show two sharp decreases in weight; one at ~280 °C and another at ~520 °C. The initial weight loss below 200 °C could be attributed to the loss of adsorbed water while the sharp weight loss at 280 °C is due to degradation of phosphoric acid.[48] The sharp decrease

at ~520 °C could be ascribed to the combined loss of excess phosphate phase in the TPP as evidenced by the TGA of as prepared powders and the loss of binding perflouorosulfonic acid polymer as perfluoro backbone is known to degrade at this temperature (Fig. S11).[49, 50] The PA content for all the TPP-Nafion® composite membranes where PA is incorporated in the slip formation ranged between 33 – 40 wt% as observed from TGA. This small variation could possibly be due to variation in excess phosphate phase of the starting TPP powders. Further doping of these membranes by imbibing in PA for 24 hours did not result in significant increase in PA doping as seen in Fig. S12, indicating that these membranes are highly in-situ doped by PA during slip formation. Nevertheless, this step was continued in all membrane fabrication process to maintain uniformity in preparation process. The in-situ doping resulted in a 50 wt% PA doping and the photographic image of the cast membrane is provided in Fig. S13. In comparison, the membranes where no PA was used in the slip formation, the PA content reached only half of that even after external PA doping for five days as observed from TGA measurements (Fig. S10). Phosphoric acid doping is observed to be essential for the conductivity of the composite membranes as composite membranes prepared without the PA doping showed conductivities of less than 10 mS cm^{-1} at 200 °C and did not provide any meaningful fuel cell performance. In comparison, the TPP-DAP membrane externally doped in PA for five days showed a conductivity of 35 mS cm^{-1} at 220 °C whereas the conductivity of in-situ PA doped TPP-DAP was 64 mS cm^{-1}. The influence of morphology on the membrane conductivity is discussed in the next section.

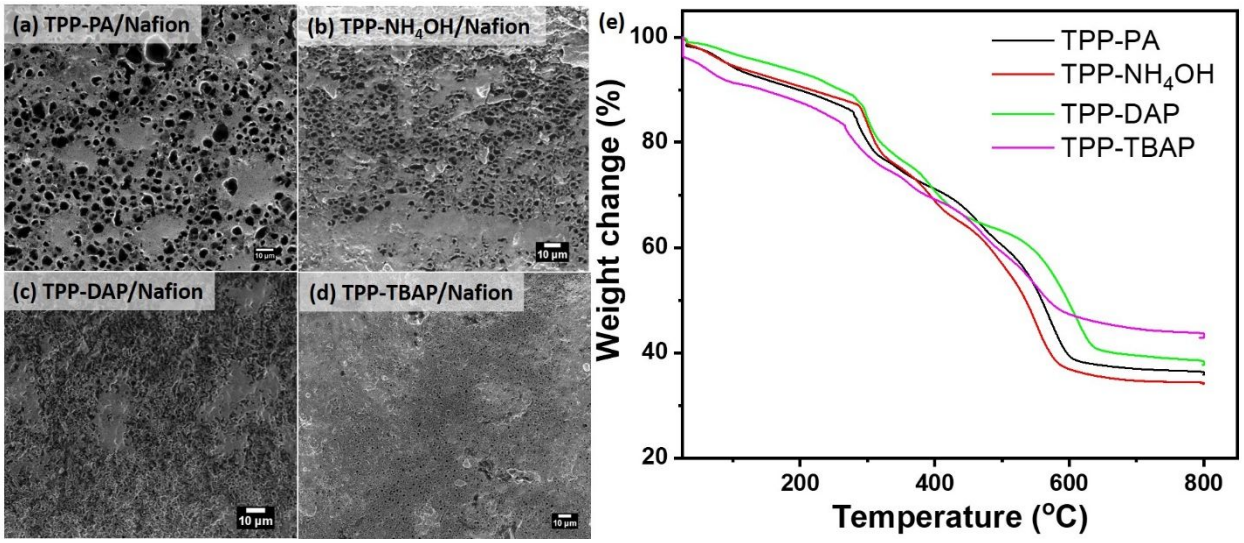

Fig. 3 SEM images of 90:10 TPP:Nafion® composite membranes prepared with (a) TPP-PA, (b) TPP-NH_4OH, (c) TPP-DAP, (d) TPP-TBAP, (e) TGA of the composite membranes prepared with 30 wt% PA added in the slip formation.

Polarization Measurements

Fuel cell polarization measurements were carried out at 220 °C with less than 1% relative humidity applied on both sides and flow rates of H_2 and O_2 maintained at 500 sccm with a back pressure of 285 kPa. A minimal humidification of < 1% is set during fuel cell operation and during conductivity measurements since SnP_2O_7 based proton conductors have been reported to show significant increase in conductivity under a P_{H_2O} of 0.12 atm.[7] An OCV of 0.98V was obtained for the TPP-TBAP/Nafion® membrane composite while other compositions generally showed OCVs lower than 0.9 V. This clearly indicates that the TPP-TBAP/Nafion® composites formed dense membranes as evidenced further by its SEM image (Fig. 3d) while other precursors formed a porous membrane that could lead to severe hydrogen cross-over and lower OCVs. This is in-line with previous reports on these type of composite membranes where despite high Peak Power Densities (PPDs) all the MEAs tested showed OCVs less than 0.9 V.[34] TPP-PA based composite membrane showed the lowest performance (PPD = 225 mW cm^{-2}) among the four tested TPP-

Nafion® composites despite having a high pellet conductivity. This is consistent with the highest porosity (35.26%) exhibited by these membranes which actually affected the resistance (higher HFR) of membrane in addition to the increased gas cross over and lower OCVs. The performance of the composite membranes increases with decreasing particle size and TBAP based composite membrane showed a PPD of 355 mW cm^{-2} that correlates well with its high pellet conductivity. The IR corrected polarization curves indicate similar polarization curves for all tested composite membranes indicating that the improved performance obtained is due to improvements in membrane characteristics and not due to variations in electrode fabrication (Fig. S14). Thus, a simple variation in the TPP powder fabrication procedure has helped to increase the fuel cell PPD by more than 50% (From 225 to 355 mW cm^{-2}). Further, the 320 mW cm^{-2} PPD obtained with TPP-DAP based membrane correlates well with the 250 mW cm^{-2} reported earlier for this type of membrane where TPP-Nafion® was also used as an ionomer in the catalyst layer.[34] In an effort to improve the fuel cell performance, we prepared a thin (~50 μm) TPP-TBAP-Nafion® composite membrane and measured its fuel cell polarization performance. Reducing the thickness of the electrolyte from ~200 μm to ~50 μm helped increase the power density of the fuel cell from 355 mW cm^{-2} to 630 mW cm^{-2} in line with the reduced ASR and agrees well with earlier reports on TPP membranes. For example, a 1.2 mm thick TPP electrolyte gave a maximum PPD of 152 mW cm^{-2} that was enhanced to 264 mW cm^{-2} upon reducing the electrolyte thickness to 0.35 mm.[9] Despite a thinner membrane, the OCV remained high (0.98 V) reconfirming the ability of TPP prepared from TBAP to form denser membranes. The comparatively smaller particle sizes (~200 nm) obtained from TPP-TBAP could have helped achieve this as polymer-ceramic composites prepared with smaller ceramic particle sizes are known to result in better performing membranes.[51] The denser membranes should result in reduced H_2 crossover as well and to verify

this we carried out linear sweep voltammetry (LSV) measurements on the four tested MEAs (Fig. S15). While LSV measurements are considered best suited for studying crossover currents, there is not much study available for this type of composite membrane under intermediate temperature operation. Hence, we used the current at 0.4 V as H_2 crossover current adapted from literature **(Please include Pucheng Pei et al., "Improved methods to measure hydrogen crossover current in proton exchange membrane fuel cell" Applied Energy, 215, 2018, 338 in the reference list here).** TPP-TBAP-Nafion® composite membrane based MEA showed the lowest H_2 crossover current of 8 $mAcm^{-2}$ at 0.4 V while TPP-PA showed a maximum crossover current of 25 $mAcm^{-2}$. This is in line with the observation of the highly porous membrane obtained with TPP-PA and dense membrane obtained for TPP-TBAP. The crossover current obtained for TPP-TBAP-Nafion® is about three times higher than that normally obtained for Nafion® 212 based membranes measured under room temperature operation. The higher crossover current value could in part be attributed to the intermediate temperature operation at 220 °C. The impedance Nyquist plots measured at various current biases during the polarization measurements and its equivalent circuit fit analysis are given in Fig. S16 and Table S1. Impedance measured at all current biases shows only a single semi-circle indicating the charge transfer resistance in the catalyst layer. It should be noted that there is no increase in mass transport resistance even at a current density of 1.8 A cm^{-2}, demonstrating the advantage of intermediate temperature fuel cells where liquid water flooding is not an issue. Further, the width of the arc decreases from 0.2 Acm^{-2} current bias to higher current biases consistent with the Butler Volmer kinetics of the oxygen reduction reaction. Nevertheless, no further increase in the width of high frequency arc is observed with increasing current biases demonstrating negligible contribution from mass transfer restrictions relating to oxygen concentration drop, that is consistent with the use of oxygen instead of air.[52] The results

observed in the polarization measurements are in accordance with in situ proton conductivity results obtained from impedance spectroscopy as provided in Table 1. The membranes formed with higher particle sizes (TPP-PA – 500 µm, TPP-NH_4OH – 220 µm) formed porous membranes and as a result showed lower proton conductivity than the TPP pellets while TPP-TBAP formed denser membranes and showed higher proton conductivity. This higher proton conductivity coupled with reduced hydrogen crossover has helped achieve significantly improved fuel cell performances. We also carried out preliminary durability measurements for one of the composite membranes where the cell was maintained at 0.5 V and polarization measurements were taken at an interval of 20 hours. The results clearly show durable performance for 90 hours of operation and an OCV >0.95 V was maintained throughout the operation (Fig. S17).

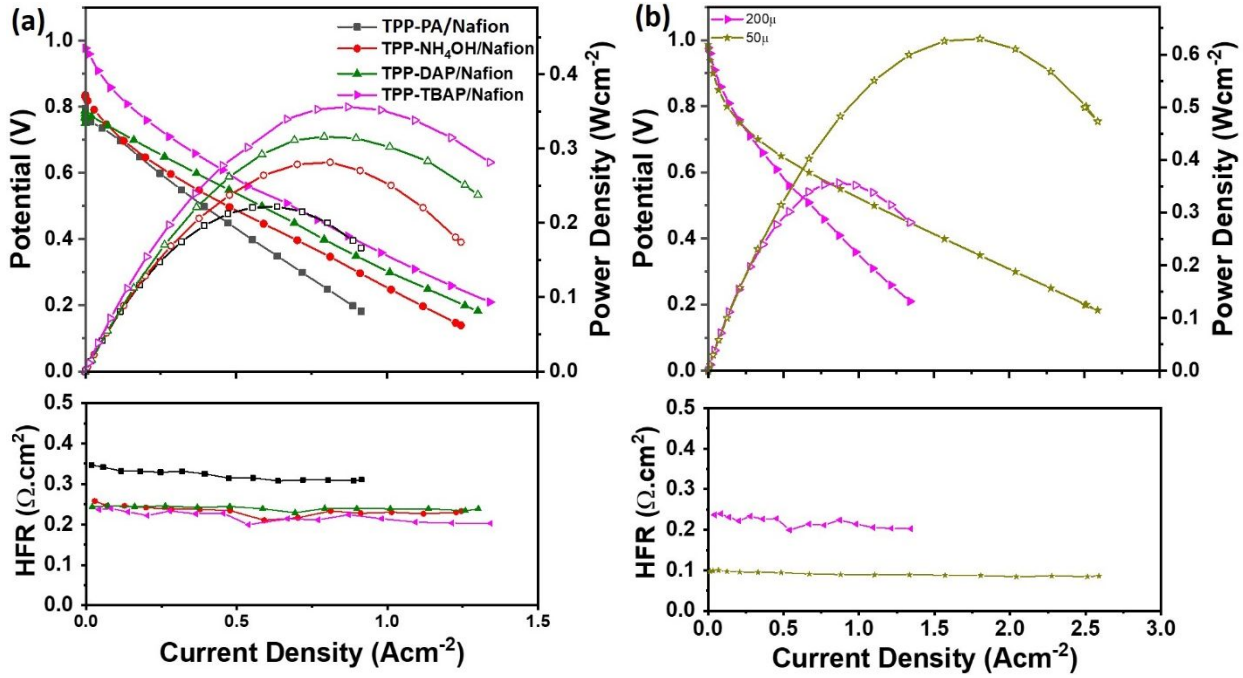

Fig. 4 (a) Fuel cell polarization and powder density plots along with HFR obtained for the four composite membranes prepared from different TPP powders, (b) Fuel cell polarization and powder density plots along with HFR obtained for TPP-TBAP/Nafion® composite membrane with two different thicknesses.

Despite significant research, metal pyrophosphate-based electrolytes have provided PPDs mostly below 300 mW cm^{-2} as summarized in Table 2 where various MPPs and their reported conductivity and PPDs are listed. While ceramic rich composites were rarely reported, MPPs have been reported to increase the fuel cell performance of PA doped PBI membranes upon doping at concentrations lower than 50 wt%. For example, at similar PA doping levels, PBI membrane alone provided a PPD of 450 mW cm^{-2} whereas incorporation of 20 wt% $Sn_{0.8}Sb_{0.2}P_2O_7$ resulted in a PPD of 670 mW cm^{-2}.[31] A similar increase in performance was recently reported for a PBI/$Ce_{0.9}Gd_{0.1}P_2O_7$ composite where the PPD was improved from 179 mW cm^{-2} for pristine PBI to 255 mW cm^{-2} for the composite membrane operating at 160 °C which was further improved to 307 mW cm^{-2} upon incorporation of graphite oxide.[32] These results clearly indicate the role of dopants with significantly higher inherent proton conductivity in enhancing the composite electrolyte's fuel cell performance. Our results on the contrary, demonstrate a ceramic rich composite (90:10 ceramic:polymer ratio) that has provided one of the highest PPDs obtained for this type of material. Further, we achieved better control over the particle size distribution with our choice of phosphate precursor that helped to form denser membranes. This has resulted in achieving higher OCVs as TPP-TBAP which showed the smallest particle sizes amongst the five prepared TPP powders, formed denser membranes resulting in OCV of 0.98 V; which is higher than all previous reports where reported OCVs were less than 0.9 V.[34] TPP ceramic powders normally show a very low surface area of less than 5 $m^2 g^{-1}$ [53] and our efforts to measure the BET surface area also resulted in very low surface areas <1 $m^2 g^{-1}$ that is possibly due to the presence of amorphous phosphate layer. Hence, we could not make a correlation between surface area of the TPP powder and membrane density and its possible role in enhancing the OCV. Nevertheless, TPP-Nafion composites have shown significant promise and our group has previously demonstrated successful

scaling up of this process in collaboration with an industrial partner, Ceramatec Inc. Hence the improvements achieved in this work will assist in furthering this type of composite materials.

Table 2 Conductivity and peak power density (PPD) reported in the literature for various metal pyrophosphates for the past 15 years (* conductivity and PPD are not reported at the same temperature, NA – not available in the mentioned reference).

Electrolyte	Temperature (°C)	Conditions	PPD (mW cm^{-2})	Conductivity (S cm^{-1})	Year[Ref]
$Sn_{0.9}In_{0.1}P_2O_7$	250	H_2/Air	264	1.95 x 10^{-1}	2006[9]
CeP_2O_7	200	H_2/O_2	25	NA	2008[54]
$Sn_{0.8}Sb_{0.2}P_2O_7$	300	Air	NA	1.00 x 10^{-1}	2008[20]
$Sn_{0.92}In_{0.08}(P_2O_7)_{1-\delta}$	900	Air	NA	6.50 x 10^{-6}	2009[35]
SnP_2O_7	175	Wet H_2	NA	2.17 x 10^{-2}	2010[21]
$Ce_{0.9}Mg_{0.1}P_2O_7$	240	H_2/Air	40	4.00 x 10^{-2*}	2011[18]
PBI/45wt.% $Sn_{0.95}Al_{0.05}P_2O_7$	200	H_2/O_2	439	3.20 x 10^{-2}	2011[39]
PBI/20wt.% $Sn_{0.8}Sb_{0.2}P_2O_7$	175	H_2/O_2	670	1.00 x 10^{-1}	2011[31]
$Sn_{0.94}Sc_{0.06}P_2O_7$	150	H_2/Air	25	NA	2011[22]
$Sn_{0.9}$ $Zn_{0.1}P_2O_{7-\delta}$	600	Air	NA	2.84 x 10^{-6}	2011[12]
$Sn_{0.91}Zn_{0.09}P_2O_{7-\delta}$	600	Wet H_2	NA	1.91 x 10^{-4}	2012[55]
$Sn_{0.9}In_{0.1}P_2O_7$	200	H_2/Air	44	NA	2012[23]
$Ce_{0.9}Mg_{0.1}P_2O_7$	90	Wet Air	NA	7.60 x 10^{-3}	2013[19]
$Sn_{0.88}Mn_{0.12}P_2O_7$	190	Wet Air	NA	2.29 × 10^{-3}	2014[56]
$Ce_{0.9}Gd_{0.1}P_2O_7$	170	Wet Air	NA	5.10 x 10^{-2}	2015[57]
CeP_2O_7/BPO_4/GO	250	5%H_2/Air	240	14.0 x 10^{-2}	2016[58]
$Zr_{0.9}Mn_{0.1}P_2O_7$	750		NA	9.09 c 10^{-5}	2016[59]
$Ti_{0.9}Mn_{0.1}P_2O_7$	180	Wet Air	NA	6.55 x 10^{-4}	2017[25]
$Sn_{0.9}In_{0.1}P_2O_7$-Li_2CO_3	630	Air	NA	5.50 x 10^{-2}	2017[60]
$Sn_2P_2O_7$/Nafion with quaternary ammonium – polystyrene ionomer	240	H_2/O_2	870	60.0 x 10^{-2}	2018[34]

$Sn_2P_2O_7$/Nafion – TPP/Nafion ionomer	240	H_2/O_2	250	60.0 x 10^{-2}	2018[34]
$Ce_{0.9}Mg_{0.1}P_2O_7$-PmOn	190	Wet Air	NA	6.21 x 10^{-2}	2018[61]
PBI/31wt.%$Ce_{0.9}Gd_{0.1}P_2O_7$/ GO	160	H_2/Air	307	19.9 x 10^{-1}*	2018[32]
SnP_2O_7/10wt.%Nafion	**220**	**H_2/O_2**	**630**	**95.0 x 10^{-2}**	**This work**

Conclusion

We have discussed the role of five different precursors on TPP synthesis and its impact on the powder morphology, crystalline phase formation, and proton conductivity. While all five precursors produced TPP with cubic Pa-3 symmetry structure, their appearance and morphology varied significantly based on the precursor. The carbon rich TMAP and TBAP precursors produced black and grey powders respectively while the other three precursors produced clear white powders. The addition of oxalic acid in the preparation stage did not affect the appearance of the powders as it has a very low burn out temperature (< 200 °C). Nevertheless, TBAP and TMAP with higher degradation temperature, assisted in forming smaller TPP particles. Therefore, TPP prepared from TBAP as a precursor exhibited a maximum conductivity of 88 mS cm^{-1} despite not having the maximum P:M ratio among the prepared TPP powders. Further, TPP from TBAP also formed denser composite membranes with Nafion®, showed lower hydrogen cross-over currents as evidenced from LSV results and as a result the TPP-TBAP/Nafion® composite membrane showed the maximum OCV (0.98 V) and PPD of 630 mW cm^{-2}, significantly higher than the PPD obtained with other precursors. Our results clearly show a way for improving the proton conductivity and fuel cell performance of TPP based intermediate temperature proton conductors by carefully choosing the phosphate precursor to control the membrane properties. Nevertheless, further research is needed to identify the precise role of precursors with a higher degradation

temperature on resulting TPP's morphology and further optimizing proton conductivity and fuel cell performance.

Experimental

Materials

All the materials mentioned below were purchased and used as received without further purification. Nafion® membranes (NR-212, 50 μm thickness) were purchased from Ion Power, Inc. (USA). Pt/C (60%, HiSPECs 9100), was purchased from Alfa Aesar (USA). Single-side ELATs gas diffusion layers (GDLs) were obtained from ETEK (USA). $SnCl_4.5H_2O$, diammonium phosphate (DAP), 1,2-pentanediol, and phosphoric acid (85 wt% in H_2O) were purchased from Sigma-Aldrich. $SnSO_4$, oxalic acid, tetrabutylammonium phosphate (TBAP), Tetra methyl ammonium sulfate, 30% NH_4OH were purchased from Alfa Aesar (USA). Deionized water and analytical grade isopropyl alcohol were used during the TPP synthesis and catalyst ink fabrication.

Synthesis of TPP powder

The TPP powders were prepared by solution precipitation method. A total of five different phosphate precursors were used for TPP synthesis while $SnSO_4$ and $SnCl_4$ were used as the metal precursor. The precursor details along with heating and drying procedure for each individual precursor case is given in Table 3. The P:M ratio of the starting material were kept close to 4.0 to accommodate some phosphate loss during sintering. In short, the precursors were mixed in 0.5 M H_2SO_4/isopropyl alcohol and heated with stirring to form a homogeneous mixture which was heated further with constant stirring until forming a frothy solid. This was dried in an air oven at 140 °C when $SnSO_4$ was used and at 60 °C for $SnCl_4$ based synthesis. 140 °C was used for initial drying process due to use of sulfuric acid. In the case of TBAP as phosphate precursor, the heating

resulted in a colorless gel that was freeze dried overnight. The solid obtained at the end of the respective drying process was calcined at 650 °C for 2.5 hours in a covered crucible. The use of covered crucible, sintering temperature and time has been optimized by our group to provide maximum P:M ratio while forming no impurity peaks. Increasing the sintering temperature or time has resulted in reduced P:M ratios and lower proton conductivities. The first three procedures involving non-carbon phosphate sources resulted in a white powder while 4 and 5 resulted in black and grey powders respectively.

Table 3. The material combination and synthesis procedure for TPP with different phosphate precursors

Phosphate precursor	Sn precursor	Heating Process	Drying process
10g 85% phosphoric acid	5g $SnSO_4$ + 5g Oxalic acid + 25 ml 0.5M H_2SO_4	Mixed at 80 °C under constant stirring	Dried at 140 °C overnight
10g 85% phosphoric acid + 15 ml 30% NH_4OH	5g $SnSO_4$ + 5g Oxalic acid + 25 ml 0.5M H_2SO_4	Mixed at 80 °C under constant stirring	Dried at 140 °C overnight
10.1g Diammonium phosphate	6.2g $SnCl_4$ + 30 ml Isopropyl alcohol	Mixed at 60 °C under constant stirring	Dried at 80 °C overnight
15g Tetramethylammonium sulphate + 10g 85% Phosphoric acid	5g $SnSO_4$ + 5g Oxalic acid + 25 ml 0.5M H_2SO_4	Mixed at 80 °C under constant stirring	Dried at 140 °C overnight
25g Tetrabutylammonium phosphate in 50ml H2O	6.2g $SnCl_4$ +30 ml Isopropyl alcohol	Mixed at 80 °C under constant stirring	Freeze drying overnight.

TPP-Nafion® composite membrane preparation

TPP-Nafion® composite membranes were fabricated by a previously reported procedure by our group.[34] The commercial Nafion® 112 membrane was exchanged with Na^+ by boiling in 1M NaOH for 1 hour followed by washing and drying at 60 °C overnight. Thus, obtained Nafion® was dissolved in pentane diol to prepare a 5 wt% solution. 1.35 g of TPP, 3 g of 5% Nafion® solution, and 0.9 g of 85% PA were mixed by a probe sonicator for 1 hour. The resulting mixture was degassed at room temperature in a vacuum chamber for 10 minutes. The resulting thick slurry was casted on a glass plate in an oven preheated to 120 °C and maintained for three hours followed by increasing the temperature to 160 °C. After reaching 160 °C, vacuum was applied and maintained for four hours. Thus obtained membranes were further doped with PA by imbibing in 85% PA for a minimum of 24 hours. For the fabrication of thin TPP-TBAP/Nafion® membranes, the slip obtained after degassing was cast on a glass plate using a doctor blade where a 500 micrometer gap was maintained that resulted in 50 μm thick membranes.[39]

Conductivity measurements on TPP powder

Pellets were obtained by pressing TPP powders in a 1.3 cm die uniaxially at 3000 psi. The pellets were sandwiched between two Pt-foil electrodes in a standard spring-loaded compression set-up. The compression set-up was placed inside a quartz tube and loaded into a tube furnace for measuring conductivity as a function of temperature. Impedance measurements were made between 1 MHz - 1 Hz using a Par4000. The high frequency intercept was used to calculate the conductivity.

Fuel cell measurements

The catalyst inks for MEA fabrication were formed by mixing 10 mg of 60% Pt/C, 20 mg of 5 wt% PWN94 ionomer solution, and 2500 mg of 80/20 IPA/water mixture by ultrasonication for an hour.

The prepared catalyst inks were painted on an ELAT GDL (5 cm^2) mounted on a vacuum plate at 60 °C and the final catalyst loading was maintained at 0.6 mg_{Pt} cm^{-2}. Prior to assembly, the electrodes were immersed in 85% phosphoric acid for 5 minutes followed by sandwiching the membrane with the two electrodes to form the MEA. A compression of 30 psi was used while assembling the single cell. Fuel cell measurements were carried out in H_2/O_2 environment using a fuel cell test station (Fuel Cell Technologies, Inc.). Polarization curves were measured between 200 – 240 °C under 1% humidification. H_2 and O_2 were supplied at a rate of 500 sccm and the cell was operated under a back pressure of 285 kPa. HFR of the cells was measured by a built-in frequency response analyzer in the frequency range of 10 kHz to 1 Hz at an amplitude of 10 mA.

Material characterization

XRD patterns were measured using a Siemens Model D5000 diffractometer with Cu Ka radiation and a graphite diffracted beam monochromator. The data was analyzed using MDI JADE Whole Profile refinement software. Thermal analysis was carried out using a Netzsch STA 449C thermogravimetric analyzer.

BET Surface Areas

A Micromeritics 3Flex instrument was used to collect the multipoint BET specific surface area (SSA). Krypton was used as the adsorbate, and liquid argon was used for the bath in all BET analyses. The samples, ranging in mass from 300 to 400 milligrams, were loaded into 19 mm glass tubes and were conditioned under vacuum at room temperature until isobaric conditions were reached (constant $\leq 1 \times 10^{-5}$ mmHg). The drying, or outgassing time before analysis was 15 days.

Acknowledgements

The authors would like to thank Dr. Juan H. Leal for performing the BET measurements. The authors thank FCTO (project ID FC180) for funding this work and Triad National Security, LLC, Operator of Los Alamos National Laboratory under U.S. Department of Energy Contract Number 89233218CNA000001 for providing the lab space to carry out the research work.

References

1. T. Norby, *Nature*, 2001, **410**, 877-878.
2. K. Scott, C. Xu and X. Wu, *Wiley Interdisciplinary Reviews: Energy and Environment*, 2014, **3**, 24-41.
3. Y. S. Kim and K.-S. Lee, *Polymer Reviews*, 2015, **55**, 330-370.
4. K.-S. Lee, J. S. Spendelow, Y.-K. Choe, C. Fujimoto and Y. S. Kim, *Nature Energy*, 2016, **1**, 16120.
5. Q. Li, J. O. Jensen, R. F. Savinell and N. J. Bjerrum, *Progress in Polymer Science*, 2009, **34**, 449-477.
6. A. S. Lee, Y.-K. Choe, I. Matanovic and Y. S. Kim, *Journal of Materials Chemistry A*, 2019, **7**, 9867-9876.
7. M. Nagao, T. Kamiya, P. Heo, A. Tomita, T. Hibino and M. Sano, *Journal of The Electrochemical Society*, 2006, **153**, A1604-A1609.
8. Y. Jin, Y. Shen and T. Hibino, *Journal of Materials Chemistry*, 2010, **20**, 6214-6217.
9. M. Nagao, A. Takeuchi, P. Heo, T. Hibino, M. Sano and A. Tomita, *Electrochemical and Solid-State Letters*, 2006, **9**, A105-A109.
10. O. Paschos, J. Kunze, U. Stimming and F. Maglia, *Journal of Physics: Condensed Matter*, 2011, **23**, 234110 (234111-234126).
11. C. R. Kreller, H. H. Pham, M. S. Wilson, R. Mukundan, N. Henson, M. Sykora, M. Hartl, L. Daemen and F. H. Garzon, *The Journal of Physical Chemistry C*, 2017, **121**, 23896-23905.
12. S. R. Phadke, C. R. Bowers, E. D. Wachsman and J. C. Nino, *Solid State Ionics*, 2011, **183**, 26-31.
13. C. R. Kreller, M. S. Wilson, R. Mukundan, E. L. Brosha and F. H. Garzon, *ECS Electrochemistry Letters*, 2013, **2**, F61-F63.
14. W. Li, A. B. Bose and I. A. Rusakova, *Journal of Power Sources*, 2016, **307**, 146-151.
15. T. Hibino, Y. Shen, M. Nishida and M. Nagao, *Angewandte Chemie International Edition*, 2012, **51**, 10786-10790.
16. J. Terasaka, K. Toyoura, A. Nakamura and K. Matsunaga, *Journal of Materials Chemistry A*, 2015, **3**, 11905-11911.
17. T. Hibino and K. Kobayashi, *Journal of Materials Chemistry A*, 2013, **1**, 6934-6941.
18. M.-V. Le, D.-S. Tsai, C.-Y. Yang, W.-H. Chung and H.-Y. Lee, *Electrochimica Acta*, 2011, **56**, 6654-6660.
19. B. Singh, S.-Y. Jeon, H.-N. Im, J.-Y. Park and S.-J. Song, *Journal of Alloys and Compounds*, 2013, **578**, 279-285.
20. X. Wu, A. Verma and K. Scott, *Fuel Cells*, 2008, **8**, 453-458.
21. H. Wang, J. Xiao, Z. Zhou, F. Zhang, H. Zhang and G. Ma, *Solid State Ionics*, 2010, **181**, 1521-1524.
22. H. Wang, H. Zhang, G. Xiao, F. Zhang, T. Yu, J. Xiao and G. Ma, *Journal of Power Sources*, 2011, **196**, 683-687.

23. P. Heo, T. Y. Kim, J. Ha, K. H. Choi, H. Chang and S. Kang, *Journal of Power Sources*, 2012, **198**, 117-121.
24. V. Nalini, R. Haugsrud and T. Norby, *Solid State Ionics*, 2010, **181**, 510-516.
25. B. Singh, A. Bhardwaj, S. K. Gautam, O. Parkash, D. Kumar, H. S. Jadhav and S.-J. Song, *Ionics*, 2017, **23**, 1675-1684.
26. Y. Li, T. Kunitake, Y. Aoki and E. Muto, *Advanced Materials*, 2008, **20**, 2398-2404.
27. V. Nalini, K. Amezawa, W. Xing and T. Norby, *Journal of The Electrochemical Society*, 2010, **157**, B1491-B1498.
28. S. Y. Gómez, F. Farzan, R. H. C. Castro and D. Hotza, *Processing, Properties, and Design of Advanced Ceramics and Composites: Ceramic Transactions Series*, 2016, **259**, 153-158.
29. H. Wang, L. Sun, J. Chen, C. Luo and S. Fan, *Ceramics International*, 2014, **40**, 3743-3746.
30. P. Babilo, T. Uda and S. M. Haile, *Journal of Materials Research*, 2007, **22**, 1322-1330.
31. X. Wu, M. Mamlouk and K. Scott, *Fuel Cells*, 2011, **11**, 620-625.
32. B. Singh, N. Devi, A. K. Srivastava, R. K. Singh, S.-J. Song, N. N. Krishnan, A. Konovalova and D. Henkensmeier, *Journal of Power Sources*, 2018, **401**, 149-157.
33. Y. C. Jin, M. Okada and T. Hibino, *Journal of Power Sources*, 2011, **196**, 4905-4910.
34. K.-S. Lee, S. Maurya, Y. S. Kim, C. R. Kreller, M. S. Wilson, D. Larsen, S. E. Elangovan and R. Mukundan, *Energy & Environmental Science*, 2018, **11**, 979-987.
35. S. Tao, *Solid State Ionics*, 2009, **180**, 148-153.
36. R. Lan and S. Tao, *Journal of Alloys and Compounds*, 2009, **486**, 380-385.
37. M. L. Einsla, R. Mukundan, E. L. Brosha and F. H. Garzon, DOI: 10.1149/1.2780948, ECS, 2007.
38. M. Einsla, R. Mukundan, E. L. Brosha and F. H. Garzon, *ECS Transactions*, 2008, **16**, 2165-2170.
39. Y. C. Jin, M. Nishida, W. Kanematsu and T. Hibino, *Journal of Power Sources*, 2011, **196**, 6042-6047.
40. C.-H. Huang, O. Knop, D. A. Othen, F. W. D. Woodhams and R. A. Howie, *Canadian Journal of Chemistry*, 1975, **53**, 79-91.
41. N. Mahato, A. Banerjee, A. Gupta, S. Omar and K. Balani, *Progress in Materials Science*, 2015, **72**, 141-337.
42. F. Fischer, G. Scholz, L. Batzdorf, M. Wilke and F. Emmerling, *CrystEngComm*, 2015, **17**, 824-829.
43. B. Ilki, S. Petrovska, R. Sergiienko, T. Tomai, E. Shibata, T. Nakamura, I. Honma and Y. Zaulychnyy, *Journal of Nanoscience and Nanotechnology*, 2012, **12**, 8913-8919.
44. K. Krishnamoorthy, M. Veerapandian, K. Yun and S. J. Kim, *Carbon*, 2013, **53**, 38-49.
45. A. Akbari, P. Sheath, S. T. Martin, D. B. Shinde, M. Shaibani, P. C. Banerjee, R. Tkacz, D. Bhattacharyya and M. Majumder, *Nature Communications*, 2016, **7**, 10891.
46. M. W. Weatherburn, *Analytical Chemistry*, 1967, **39**, 971-974.
47. D. Aili, M. K. Hansen, C. Pan, Q. Li, E. Christensen, J. O. Jensen and N. J. Bjerrum, *International Journal of Hydrogen Energy*, 2011, **36**, 6985-6993.
48. C. Liu, S. B. Khan, M. Lee, K. I. Kim, K. Akhtar, H. Han and A. M. Asiri, *Macromolecular Research*, 2013, **21**, 35-41.
49. R. Sigwadi, M. S. Dhlamini, T. Mokrani, F. Ṇemavhola, P. F. Nonjola and P. F. Msomi, *Heliyon*, 2019, **5**, e02240.
50. R. Kannan, B. A. Kakade and V. K. Pillai, *Angewandte Chemie International Edition*, 2008, **47**, 2653-2656.
51. T. Hanemann and D. V. Szabó, *Materials*, 2010, **3**.
52. T. E. Springer, T. A. Zawodzinski, M. S. Wilson and S. Gottesfeld, *Journal of The Electrochemical Society*, 1996, **143**, 587-599.
53. W. H. J. Hogarth, S. S. Muir, A. K. Whittaker, J. C. Diniz da Costa, J. Drennan and G. Q. Lu, *Solid State Ionics*, 2007, **177**, 3389-3394.

54. X. Sun, S. Wang, Z. Wang, X. Ye, T. Wen and F. Huang, *Solid State Ionics*, 2008, **179**, 1138-1141.
55. J. Xiao, H. Zhang, Z. Yang, H. Wang, G. Ma and Z. Zhou, *Journal of Alloys and Compounds*, 2012, **521**, 106-111.
56. B. Singh, J.-H. Kim, J.-Y. Park and S.-J. Song, *Journal of the European Ceramic Society*, 2014, **34**, 2967-2976.
57. B. Singh, J.-H. Kim, J.-Y. Park and S.-J. Song, *Ceramics International*, 2015, **41**, 4814-4821.
58. X. Huang, Y. Deng, C. Xu, Y. Hu, L. Yang, P. Luo, Y. Lu and J. Cheng, *Fuel*, 2016, **179**, 299-304.
59. B. Singh, J.-H. Kim, O. Parkash and S.-J. Song, *Ceramics International*, 2016, **42**, 2983-2989.
60. B. Singh, A. Bhardwaj, S. K. Gautam, D. Kumar, O. Parkash, I.-H. Kim and S.-J. Song, *Journal of Power Sources*, 2017, **345**, 176-181.
61. B. Singh, N. Devi, L. Mathur, R. K. Singh, A. Bhardwaj, S.-J. Song and D. Henkensmeier, *Ceramics International*, 2018, **44**, 6170-6175.

Table of Contents

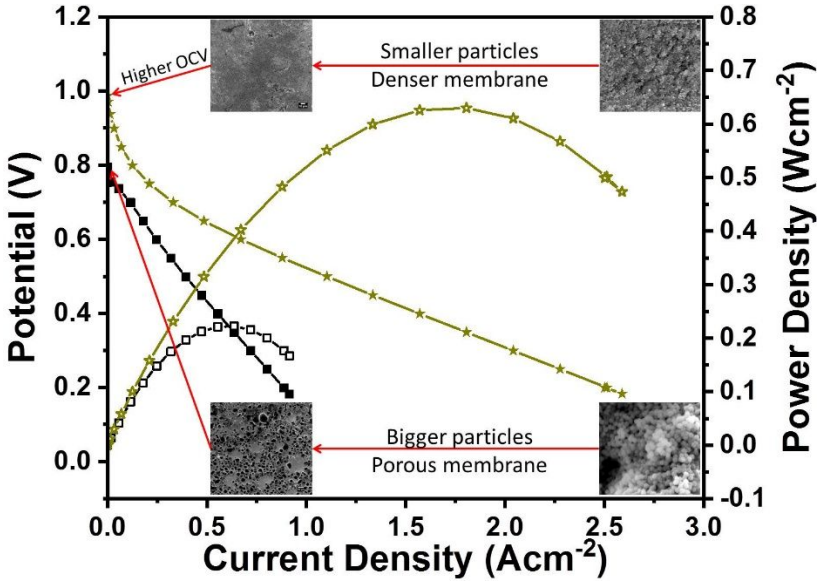

Proper phosphorus precursor selection during synthesis could help produce better tin-pyrophosphate powder and composite membranes with improved fuel cell performance.